

# Study of Short-distance Spin and Charge Correlations and Local Density-of-States in the CMR regime of the One-Orbital Model for Manganites

Rong Yu,<sup>1,2</sup> Shuai Dong,<sup>1,2,3</sup> Cengiz Şen,<sup>4</sup> Gonzalo Alvarez,<sup>5</sup> and Elbio Dagotto<sup>1,2</sup>

<sup>1</sup>*Department of Physics and Astronomy, University of Tennessee, Knoxville, TN 37996, USA*

<sup>2</sup>*Materials Science and Technology Division, Oak Ridge National Laboratory, Oak Ridge, TN 32831, USA*

<sup>3</sup>*Nanjing National Laboratory of Microstructures, Nanjing University, Nanjing 210093, China*

<sup>4</sup>*Department of Physics, University of Cincinnati, Cincinnati, OH 45221, USA*

<sup>5</sup>*Computer Science and Mathematics Division and Center for Nanophase Materials Science, Oak Ridge National Laboratory, Oak Ridge, TN 37831, USA*

The metal-insulator transition, and the associated magnetic transition, in the colossal magnetoresistance (CMR) regime of the one-orbital model for manganites is here studied using Monte Carlo (MC) techniques. Both cooperative oxygen lattice distortions and a finite superexchange coupling among the  $t_{2g}$  spins are included in our investigations. Charge and spin correlations are studied. In the CMR regime, a strong competition between the ferromagnetic metallic and antiferromagnetic charge-ordered insulating states is observed. This competition is shown to be important to understand the resistivity peak that appears near the critical temperature. Moreover, it is argued that the system is dynamically inhomogeneous, with short-range charge and spin correlations that slowly evolve with MC time, producing the glassy characteristics of the CMR state. The local density-of-states (LDOS) is also investigated, and a pseudogap (PG) is found to exist in the CMR temperature range. The width of the PG in the LDOS is calculated and directly compared with recent scanning-tunneling-spectroscopy (STS) experimental results. The agreement between our calculation and the experiment suggests that the depletion of the conductance at low bias observed experimentally is a reflection on the existence of a PG in the LDOS spectra, as opposed to a hard gap. The apparent homogeneity observed via STS techniques could be caused by the slow time characteristics of this probe. Faster experimental methods should unveil a rather inhomogeneous state in the CMR regime, as already observed in neutron scattering experiments.

PACS numbers: 75.47.Lx, 75.47.Gk, 75.30.Mb, 75.40.Mg

## I. INTRODUCTION

The colossal magnetoresistance effect in manganites continues attracting considerable interest in both condensed matter physics and material science.<sup>1,2,3,4,5</sup> Clarifying the origin of the CMR effect is expected to fundamentally contribute to our understanding of the intrinsic complexity observed in a variety of transition metal oxides. In addition, these compounds are receiving much attention for their potential application in new generations of spintronics devices.<sup>6</sup> Manganites present a very rich phase diagram with a variety of competing states, giving rise to the exotic behavior found in these compounds. To explain the CMR effect, originally a double exchange (DE) model was proposed.<sup>7</sup> However, it was shown later that the DE mechanism itself could not explain the large changes in the resistivity with increasing magnetic fields that were observed experimentally.<sup>8,9</sup> Thus, other couplings, such as the electron-phonon interactions, must be taken into account.<sup>10</sup> Subsequent investigations have shown that the existence of insulating states competing with the DE induced ferromagnetic metal, and the concomitant emergence of nanometer-scale phase separation, could be the key ingredients to understand the CMR effect.<sup>11,12,13</sup>

After the phase separation idea was proposed, a variety of theoretical studies have been reported, including calculations using simplified spin models and random

resistor networks.<sup>14,15,16</sup> More realistic one-orbital and two-orbital models, including electron-phonon coupling and quenched disorder,<sup>17,18,19,20,21</sup> have also been investigated. In several of these calculations a CMR behavior of the resistivity vs. temperature has been observed. The ferromagnetic (FM) metallic phase is commonly accepted as one of the competing states necessary for CMR. The other competitor should be an antiferromagnetic (AF) charge-ordered (CO) insulating state. But for technical reasons related with the complexity of the numerical simulations, the CMR arising from the competition between the FM metallic and the AF/CO insulating states has not been discussed in most of the efforts mentioned above. However, very recently Şen *et al.*<sup>22</sup> carefully analyzed the influence of the superexchange coupling  $J_{AF}$  between the localized  $t_{2g}$  electrons on the physical properties of both the one- and two-orbital models including cooperative oxygen lattice distortions. Two competing ground states were discovered at low temperatures: a FM metallic phase and an AF/CO insulating phase (for the charge and spin arrangement in these states see Fig. 1). These two phases are separated by first-order transitions at low temperatures. A thermal transition from either phase to a paramagnetic (PM) insulator at high temperature was also observed. Close to the bi-critical point in the phase diagram, the CMR effect in the resistivity was found.<sup>23</sup> This is a location where enhanced phase competition is observed. The CMR effect has been shown to be deeply connected with the existence of short-distance

charge correlations above the critical temperature of the thermal transition.<sup>22</sup>

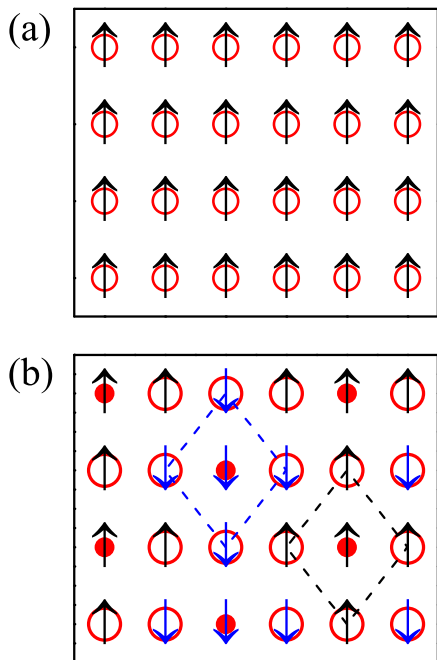


FIG. 1: (color online) The two competing ground states in the one-orbital model at electronic density  $n=0.75$ , obtained by varying the superexchange coupling  $J_{AF}$ , as explained in Ref. 22 and in the text. The FM metallic state is in (a) and the AF/CO insulating state in (b). The arrows denote the classical  $t_{2g}$  spins and the open circles are proportional to the electronic density. The full circles in (b) simply denote the location of the holes. The dashed lines in (b) define “spin blocks”, that are discussed later in the text.

In this paper, the recent effort by Şen *et al.*<sup>22</sup> is further expanded, focusing on the analysis of the phase competition in the thermal metal-insulator (MI) transition of the one-orbital model. We have observed that the development of short-range spin-spin correlations, with characteristics similar to those in the AF/CO competing state, is important to understand the CMR effect. This result supplements the previous investigations that focused on the charge sector exclusively.<sup>22</sup> The systems without quenched disorder that we study in this work are shown to be statistically homogeneous when averaged over very long MC times. However, charge localization together with robust short-distance correlations of charges and spins are observed at short MC times. This leads us to argue that a *dynamical* inhomogeneity occurs in manganites in cases where the strength of the quenched disorder is weak (namely for materials close to the clean limit).

A second purpose of our present effort is to use numerical techniques to calculate the LDOS. Since the one-orbital model has been shown to successfully describe the behavior of the resistivity in the CMR regime,<sup>22</sup> this approach should be able to explain other proper-

ties in the same temperature range. The LDOS is important to contrast theory with STS experiments, which are useful to probe local electronic structures in a variety of complex materials, possibly providing information about phase separation in manganites.<sup>24,25</sup> In fact, the derivative of the experimentally obtained current-voltage curve is directly related to the LDOS. Our calculations are even more relevant in view of recently reported puzzling STS results. In Refs. 26,27, a depletion of the conductance at low bias was observed in the *low* temperature metallic phase of both  $\text{La}_{0.77}\text{Ca}_{0.23}\text{MnO}_3$  (LCMO) and  $\text{La}_{0.350}\text{Pr}_{0.275}\text{Ca}_{0.375}\text{MnO}_3$  (LPCMO) films, implying the existence of a gapped quasi-particle excitation spectra in these materials. No coexistence of insulating and metallic regions was observed in the experiment, in apparent disagreement with existing theories. These results are very surprising since a gapped spectrum cannot lead to a metallic state. Singh *et al.*<sup>27</sup> proposed that the surface of LPCMO is different from the bulk: at the surface the AF/CO state is stable, while in the bulk a coexistence of metallic and insulating regions dominates, as shown in other experiments. We do not disagree with this proposal, and for LPCMO it may well be the solution of the puzzle. For LCMO, the same hypothesis may work, but here we propose another alternative. In our calculations reported below, a PG in the LDOS (as opposed to a gap) is found in the entire temperature range where the CMR occurs in the one-orbital model. This PG feature is known to be a signature of doped manganites and results from mixed-phase tendencies.<sup>28,29</sup> We have investigated the width of the PG and compare it with the experimentally determined gap width. We have observed a very good agreement between our calculation and the experimental results. This provides an alternative way to understand the STS data for LCMO: the experimentally observed gap could arise from a PG in the LDOS, not from a gap. Moreover, within this picture, the apparent spatial homogeneity observed in the STS experiment can be explained as a time-averaged property. The system is actually dynamically inhomogeneous, which could be experimentally detected if the time scale of the probing technique is comparable to the characteristic time of the dynamics of the system. Fast measurements (using, e.g., neutron scattering) have already shown evidence of “correlated polarons” in LCMO<sup>30</sup> in contradiction with LCMO STS experiments. Our calculations show that this is to be understood based on the dynamical nature of the CMR state: a homogeneous gap detected in STS is not in contradiction with other faster measurements, to the extent that it is understood that the gap is actually a PG in the LDOS.

This paper is organized as follows: in Sec. II, we briefly introduce the one-orbital model and the details of the MC technique that we used. In Sec. III, we focus on investigating the competition between the FM metallic and the AF/CO insulating states. Spin correlations are shown to play an important role in the system, particularly in the CMR regime. Moreover, our investigations in this section

show that the phase competition in the CMR regime is dynamic, at least within the time evolution generated by the MC procedure, which is based on local interactions. In Sec. IV, a detailed study of the PG in the LDOS of the one-orbital model is provided. We compare our results with those in the recent STS experiments, and show that their observations can be explained within our model. Conclusions are in Sec. V.

## II. THEORETICAL MODEL

In this study, the properties of the one-orbital model for manganites are analyzed using numerical techniques. Although a two-orbital model with Jahn-Teller couplings is more realistic, it is also more difficult to study computationally. In fact, using the exact diagonalization procedure for the fermionic sector, a simulation using two orbitals costs  $2^4=16$  times more CPU time than using only one orbital. Since it has been extensively shown that the one-orbital model captures the physics of phase competition in manganites,<sup>13</sup> being restricted to one orbital is not a drastic approximation. Moreover, the current effort builds upon the previous results obtained in Ref. 22, where the one-orbital model was also considered. Then, for a proper comparison, it is imperative to use the same model. The Hamiltonian reads

$$\begin{aligned}
H = & -t \sum_{\langle ij \rangle, \alpha} (d_{i,\alpha}^\dagger d_{j,\alpha} + h.c.) - J_H \sum_{i,\alpha,\beta} d_{i,\alpha}^\dagger \sigma_{\alpha,\beta} d_{i,\beta} \cdot \mathbf{S}_i \\
& + J_{AF} \sum_{\langle ij \rangle} \mathbf{S}_i \cdot \mathbf{S}_j - \lambda t \sum_{i,\delta,\alpha} (u_{i,-\delta} - u_{i,\delta}) d_{i,\alpha}^\dagger d_{i,\alpha} \quad (1) \\
& + t \sum_{i,\delta} u_{i,\delta}^2 + \sum_{i,\alpha} (\Delta_i - \mu) n_{i,\alpha},
\end{aligned}$$

where  $d_{i,\alpha}$  and  $d_{i,\alpha}^\dagger$  are the fermionic annihilation and creation operators of  $e_g$  electrons, acting on site  $i$  and with  $z$ -axis spin projection  $\alpha$ .  $\{\sigma\}$  denote the Pauli matrices.  $\mathbf{S}_i$  represents the  $t_{2g}$  spin degrees-of-freedom localized at site  $i$ . This spin is assumed to be classical, a widely used approximation also employed in Ref. 22. The first two terms in Eq. 1 correspond to the ordinary DE model. The third term introduces AF interactions between the localized  $t_{2g}$  spins. Although the coupling regulating the strength of this term is considered weak in magnitude,<sup>13</sup> previous work has shown that its presence is crucial to stabilize the AF/CO states that compete with the FM ground state resulting from the double-exchange mechanism.<sup>31</sup> The next term in the Hamiltonian contains the interaction between the mobile electrons and the cooperative phonons ( $\delta$  runs over the spatial directions). As in Ref. 22 and several other investigations, the oxygen lattice displacements  $u_{i,\delta}$  with respect to the equilibrium position are considered to be classical. These displacements are located at the links of a two-dimensional square lattice. The oxygen lattice distortions induced by the electron-phonon interaction

are further balanced by an elastic energy proportional to  $u_{i,\delta}^2$ . The last term in the Hamiltonian Eq. 1 contains the quenched on-site disorder that simulates the effect of chemical doping in real manganites. As in Ref. 22 and other publications, this disorder should enter via a randomly chosen set of values for the on-site energy  $\Delta_i$  at every site. However, although it has been shown that the quenched disorder can enhance substantially the magnitude of the CMR effect,<sup>32</sup> it has been observed<sup>22</sup> that its presence would not change the physical picture qualitatively. If quenched disorder is ignored, the only price to pay is the need to tune couplings to be very close to the first-order FM-AF/CO transition in order to observe CMR physics.<sup>22</sup> Then, for numerical simplicity, here we consider only the clean limit CMR, i.e.,  $\Delta_i = 0$  and focus on the immediate vicinity of the FM-AF/CO transition in parameter space. As a consequence, our conclusions below regarding the dynamical character of the inhomogeneities will then be of much more relevance to “clean” manganites than “dirty” ones. Finally,  $\mu$  is the chemical potential and  $n_{i,\alpha}$  is the number operator.

In the present calculation, and also for simplicity, the limit  $J_H \rightarrow \infty$  is considered. This is another of the several well-accepted approximations widely used in previous studies of theoretical models for manganites. This limit preserves the essential physics of the CMR effect. According to this approximation, the spin of the  $e_g$  electrons is always parallel to the direction of the spin of the  $t_{2g}$  electrons. Hence, the Hamiltonian is reduced to

$$\begin{aligned}
H = & -t \sum_{\langle ij \rangle} (\Omega_{ij} c_i^\dagger c_j + h.c.) + J_{AF} \sum_{\langle ij \rangle} \mathbf{S}_i \cdot \mathbf{S}_j \\
& - \lambda t \sum_{i,\delta} (u_{i,-\delta} - u_{i,\delta}) c_i^\dagger c_i \quad (2) \\
& + t \sum_{i,\delta} u_{i,\delta}^2 - \sum_{i,\alpha} \mu c_i^\dagger c_i,
\end{aligned}$$

where  $c_i^\dagger$  creates an  $e_g$  electron with spin parallel to the localized  $t_{2g}$  spin at site  $i$ . The classical localized spin can be parametrized as  $\mathbf{S}_i = (\sin \theta_i \cos \phi_i, \sin \theta_i \sin \phi_i, \cos \theta_i)$  in spherical coordinates. The influence of the infinite Hund coupling is reflected in the electron hopping term that now carries a Berry phase:<sup>3</sup>

$$\Omega_{ij} = \cos \frac{\theta_i}{2} \cos \frac{\theta_j}{2} + \sin \frac{\theta_i}{2} \sin \frac{\theta_j}{2} e^{i(\phi_i - \phi_j)}. \quad (3)$$

The Hamiltonian Eq. 2 is solved here via a standard combination of exact diagonalization of the fermionic sector and a MC evolution of the classical spin and oxygen lattice distortion degrees-of-freedom. At each MC step, the quadratic fermionic portion in the Hamiltonian is diagonalized numerically, using library subroutines, for a given configuration of classical spins and phonons. A new set of configurations for the next MC step is then generated following the Metropolis algorithm. This method has been successfully used in previous studies and details can be found in Refs. 3,11 and 13. Physical quantities can be

easily calculated as MC averages. For instance, at each MC step, the LDOS is evaluated using the eigenvalues and eigenvectors that arise from the diagonalization.<sup>13</sup> The resistivity  $\rho$  is obtained from the inverse of the average conductivity  $\sigma$ . In two dimensions (2D), where our effort focuses on, it can be shown that  $\sigma = G$ , where  $G$  is the conductance. This conductance is calculated using the Kubo formula.<sup>33</sup> In this effort, 2D systems with charge density  $n=0.75$  are studied for a proper comparison with the results in Ref. 22 that were obtained at the same density and dimensionality. The typical clusters analyzed here are of size  $8 \times 8$  and  $12 \times 12$ . If not specified, simulations start with a random configuration of spins and lattice displacements. To overcome the metastabilities caused by the dynamical inhomogeneity that appears in this study (discussed in detail in the following sections), very long MC runs were needed. In practice, up to  $10^5$  MC steps for thermalization were used, followed by  $5 \times 10^4$  steps for measurements. This was needed on the  $8 \times 8$  lattice to obtain statistically homogeneous results. For the same purpose,  $10^4$  steps for thermalization and another  $10^4$  steps for measurements were used for the  $12 \times 12$  lattice.

### III. COMPETITION BETWEEN FERROMAGNETIC AND CHARGE-ORDERED ANTIFERROMAGNETIC STATES

It has been shown<sup>22</sup> that the model Eq. 2 has two competing states at low temperatures, at the  $n=0.75$  density considered here. The ground state is a FM metal if  $J_{AF}$  is zero or very small. However, upon increasing  $J_{AF}$  an AF/CO insulator is reached via a first-order phase transition. In this insulating phase, both charges and spins are arranged in a non-homogeneous, but regular, pattern. This is significantly different from the FM state, where both charge and spin are uniformly distributed, namely they are the same at every site. At high temperatures, the system loses long-range order and it is in a paramagnetic (PM) phase. The most striking feature found in this model<sup>22</sup> is that close to the phase boundary between the FM and AF/CO states, the cooling down of the system from the high-temperature PM phase causes drastic changes in the resistivity  $\rho$ . First,  $\rho$  increases with decreasing temperature and develops a prominent peak. It then drops rapidly (about 2-3 orders of magnitude) when the system enters into the FM state. The resistivity peak can be largely suppressed by small magnetic fields, showing the so-called CMR effect.<sup>22</sup> While it is clear that the AF/CO state of the one-orbital model is not exactly as found in experiments, which are dominated by CE states that also present orbital order, the promising results for  $\rho$  vs. temperature show that the key qualitative features of the CMR effect do appear in the one-orbital model.

In this section, we will focus on the MI transition that causes the CMR, and show how this CMR effect is connected to the competition FM vs. AF/CO.

#### A. Metal-Insulator Transition and the CMR Effect

Let us first revisit the thermal transition related to the CMR effect that occurs in a narrow parameter regime of the one-orbital model.<sup>22</sup> This transition is simultaneously insulator to metal and PM to FM, upon cooling, similarly as in experiments. This MI transition and the associated magnetic transition, for a lattice of size  $12 \times 12$  and at electronic density  $n=0.75$ , are shown in Fig. 2. The critical temperature  $T_C$  of the magnetic transition is approximately located at the resistivity peak, i.e.,  $T_C \approx T_{MI}$ . At temperatures lower than  $T_{MI}$  the resistivity falls down rapidly, about two orders in magnitude within a narrow temperature window  $T/t \approx 0.01$ . A similar behavior in both the resistivity and the uniform magnetization is also observed within a relatively narrow range of parameters:  $\lambda \sim 1.1 - 1.2$  and  $J_{AF} \sim 0.02 - 0.034$ .

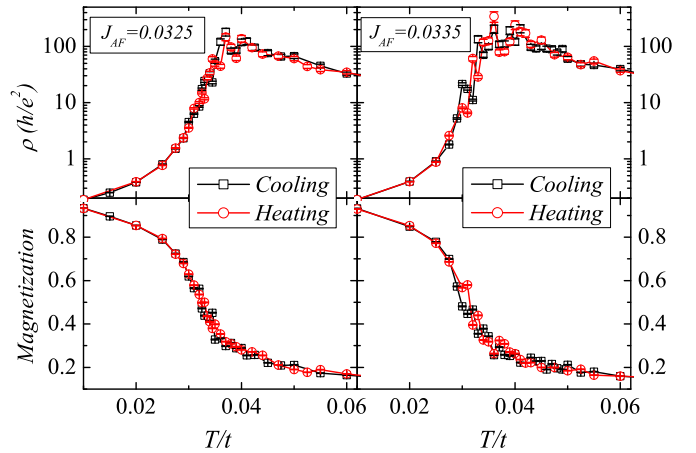


FIG. 2: (color online) Resistivity and uniform magnetization upon cooling (black) and heating (red) for  $J_{AF}=0.0325$  (left panel) and  $J_{AF}=0.0335$  (right panel). The result was obtained on a  $12 \times 12$  square lattice using  $\lambda=1.2$ , density  $n=0.75$ , and in the clean limit ( $\Delta=0$ ). No hysteresis loop is observed in both quantities.

In Fig. 2, the resistivity and uniform magnetization phase transitions were studied in the following way. For cooling, we started the MC simulation at a high temperature  $T \gg T_{MI}$  using a random spin and phonon configuration. After MC converging at the initial temperature, we started another simulation at a lower temperature by using the final configuration from the previous temperature as the new initial input. For heating, we proceeded in a similar way, but the first simulation at the lowest temperature was initialized with a perfect ferromagnetic spin configuration (note that the CMR effect occurs very close to the FM-AF/CO transition but slightly on the side of the FM phase, thus there is no need to start any simulation with the AF/CO state). Both the heating and cooling procedures were performed “slowly” in temperature. By this procedure, we can detect possible differ-

ent responses of the system upon heating and cooling, which is usually associated with the existence of first-order transitions. However, based on the results shown in Fig. 2, no hysteresis loop has been observed, either in  $\rho$  or in the magnetization. This suggests that both the MI and magnetic transitions are of second-order in this one-orbital model in the clean limit. Interestingly, our result is consistent with a recent analytical work<sup>20</sup> showing that the transition is of second-order in the absence of quenched disorder<sup>34</sup>.

### B. Short-Range Spin and Charge Correlations in the CMR Regime

The CMR regime, where the resistivity peak develops during the MI transition, is close to the bi-critical point separating the FM and AF/CO states in the clean-limit one-orbital model phase diagram.<sup>22</sup> This indicates that at low temperatures, two competing ground states with different long-range orders exist. Although by definition long-range order cannot survive above a critical temperature, in this temperature regime it is very common to find robust short-range correlations of the order that will become stable at low temperatures. This certainly occurs in the FM phase far from the region of competition with other states. However, dramatically different from this well-established concept, previous studies<sup>22</sup> observed that in the CMR regime, the short-range order that develops above the Curie temperature is in the *charge* sector. Namely, it is *unrelated with the FM state*. Moreover, the observed short-distance charge correlations are very similar to those of the competing AF/CO state. Thus, the short-distance physics above  $T_C$  near the bi-critical point is very different from the properties of the FM state, which is the actual ground state of the system.

The short-distance tendency toward a CO state above  $T_C$  and  $T_{MI}$  accounts for the appearance of the resistivity peak at  $T_{MI}$ . The system develops CO charge correlation upon cooling and this proceeds together with an increase in the resistance, since the AF/CO state is insulating. In this section, we confirm all these previous observations. More importantly, here we will also consider the short-distance spin correlations above  $T_C$ , which were not analyzed before. We will arrive to the conclusion that *both* short-distance charge and spin correlations are important in explaining the resistivity peak.

An intuitive procedure to understand the short-distance spin and charge correlations in the one-orbital model is to analyze MC “snapshots”, namely equilibrated configurations generated by the MC procedure. Examples are presented in Fig. 3. Before analyzing them, and to guide the discussion, let us first consider what are the expected “building blocks” in the charge-ordered state, and then we will investigate if these building blocks are observed in the simulations. Since it is anticipated that the short-distance behavior above  $T_C$  has strong similarities with the AF/CO competing state, the expected

building blocks, both for the one- and two-orbital models, are shown in Figs. 3 (e) and (f), respectively. In the one-orbital model, the study in Ref. 22 has shown that at  $n=0.75$  the building block consists of a hole carrier surrounded by its four neighboring sites, each carrying an electron. The five localized  $t_{2g}$  spins involved in this block have the same orientation of those spins. This block has similarities with a FM polaron, but quite contrary to a naive “FM polaron gas” scenario the AF/CO state is achieved by arranging these blocks *antiferromagnetically* in a regular pattern (see also Fig. 1(b)). For the two-orbital model, shown here only for completeness, the most likely building block should be a small segment of the well-known CE-type FM zigzag chains (see Fig. 3(f)).

It is remarkable that the building blocks of the AF/CO state of the one-orbital model can actually be observed in the MC snapshots shown in Figs. 3 (a) to (c), for a value of  $J_{AF}$  where the ground state is FM. We find that the short-range 2 and  $\sqrt{5}$  charge correlations clearly exist at short distances, in both the high-temperature insulating PM and low-temperature metallic FM phases. In the FM state, spins are almost parallel to each other, and hole hopping is allowed. This gives the FM state a metallic nature. Moreover, it will be shown below that the charge is fairly mobile at low temperature, thus effectively the building blocks lose their identity and they merge into a metallic FM state. Different is the situation at larger temperatures. When  $T \gtrsim T_{MI}$  (shown as  $T/t=0.035$  in Fig. 3), the short-distance tendency to the competing AF/CO state is significant. This tendency is further confirmed by analyzing the short-range spin-spin correlations. On one hand, the spins that are the nearest neighbors to a hole site are almost parallel to the spin on that site, indicating short-range FM correlations. On the other hand, spins localized on different hole sites prefer to align antiferromagnetically at distances  $\sqrt{5}$ , as expected from the discussion in Ref. 22. Then, the MC simulation clearly shows the presence of the building blocks described in the previous paragraph (two of them are highlighted in Fig. 3(b)). As the temperature cools down, these “preformed” building blocks rotate and orient themselves into a FM pattern. At higher temperature  $T/t=0.1$ , both short-range spin and charge correlations are much suppressed by thermal fluctuations, but the building blocks can still be identified (see Fig. 3(c)).

By monitoring the above described MC snapshots, a simple picture of the temperature evolution of the system near the bi-critical point emerges: upon cooling from high temperature, the building blocks develop, and first they start arranging in a pattern similar to the AF/CO state. This causes the insulating properties above the Curie temperature. Upon further cooling, the building blocks rotate their relative orientation from AF/CO to the FM state, rendering the state metallic. To observe this effect more explicitly, we propose an operator  $\hat{O}$  which characterizes the spin and charge correlations in the AF/CO state, and study the temperature evolution



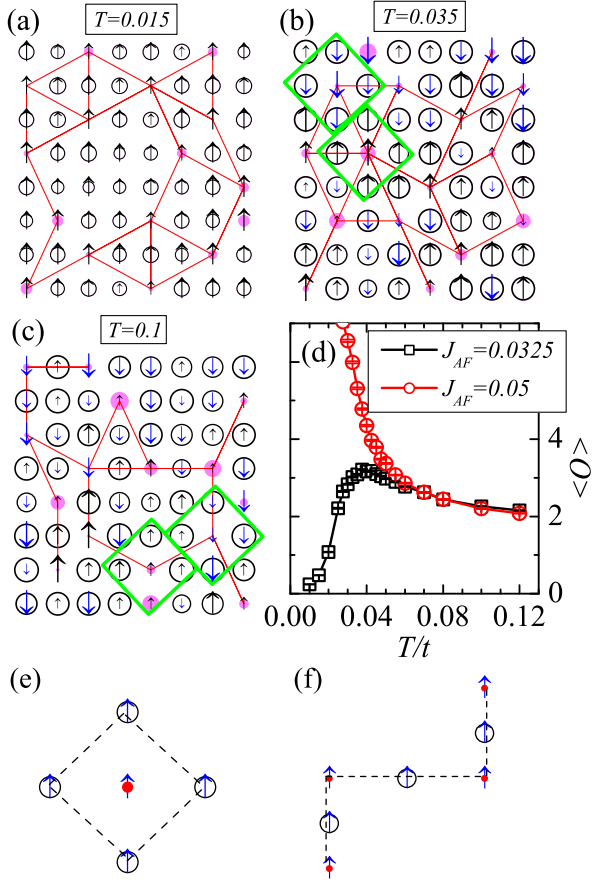


FIG. 3: (color online) (a)-(c) Typical MC snapshots of local charge density and spin correlations on a  $8 \times 8$  lattice with  $J_{AF} = 0.0325$ ,  $n = 0.75$ , and  $\lambda = 1.2$  at three different temperatures. In each snapshot, the circle radius is proportional to the local charge density. The 16 holes are represented by filled circles. The length of the arrow at each site  $i$  is proportional to the spin-spin correlation  $\langle \mathbf{S}_0 \cdot \mathbf{S}_i \rangle$ , where  $\mathbf{S}_0$  is a reference point located on a hole site. Presenting this correlation, as opposed to directly showing the classical spins, allows an easier visualization since now most spins are in the plane of the figure. Holes with  $\sqrt{5}$  and 2 correlations are highlighted, as well as a couple of well-formed building blocks (see text) at the two highest temperatures. (d) The temperature dependence of the proposed operator  $\hat{O}$  (Eq. 4). The result of  $\langle \hat{O} \rangle$  is averaged over  $5 \times 10^4$  MC steps. (e) The building block (see text) of the AF/CO state of the one-orbital model at  $n=0.75$ . (f) Proposed building block of the AF/CO state in the two-orbital model at  $n=0.5$ , for completeness.

of  $\hat{O}$  in the system. The operator is

$$\hat{O} = \sum_{\mathbf{i}, \mathbf{j}=\text{hole}} (-)^{\mathbf{i}-\mathbf{j}} \bar{\mathbf{S}}_{\mathbf{i}} \cdot \bar{\mathbf{S}}_{\mathbf{j}} (1 - n_{\mathbf{i}})(1 - n_{\mathbf{j}}), \quad (4)$$

where  $\bar{\mathbf{S}}_{\mathbf{i}} = \frac{1}{5} [\mathbf{S}_{\mathbf{i}} + \sum_{\delta} \mathbf{S}_{\mathbf{i}+\delta}]$  is the average of the classical spin of the hole site<sup>35</sup> and its four neighbors (namely, the

“spin block” region enclosed by a diamond in Fig. 1(b) or 3(e)). Note that  $\langle \hat{O} \rangle = n_{\text{hole}}^2$  in a perfect AF/CO state with  $n_{\text{hole}}$  hole carriers. This same operator vanishes in either a state with perfect FM order or in a PM state with uncorrelated randomly distributed spins.

The temperature dependences of  $\hat{O}$  for two values of  $J_{AF}$  are shown in Fig. 3(d). At  $J_{AF}/t=0.05$ , the ground state does not present long-range AF/CO order, and no resistivity peak was observed. At this  $J_{AF}$  value,  $\langle \hat{O} \rangle$  increases monotonically upon cooling and saturates to a large finite value when  $T \rightarrow 0$ . The mean-value of this operator illustrates the transition from PM to AF/CO states. Interestingly, in the CMR regime, such as for  $J_{AF}/t=0.0325$  where the FM state is the ground state,  $\langle \hat{O} \rangle$  evolves fairly differently. Upon cooling, it first slowly increases following very closely the result at  $J_{AF}/t=0.05$ , but then develops a peak at  $T \approx T_{MI}$ , and subsequently drops fast to a nearly vanishing value at the lowest temperature investigated. This non-monotonic temperature dependence clearly reflects the enhanced tendency to the AF/CO state at  $T \gtrsim T_{MI}$ , intuitively observed in the MC snapshots. Remarkably, the temperature dependence of  $\langle \hat{O} \rangle$  and the resistivity shows a qualitative similarity. It confirms that the resistivity peak in the CMR regime is simply a reflection of the short-distance tendency to the competing AF/CO state. We note that this idea has been proposed in previous studies,<sup>21,22</sup> but only the charge correlations were considered as relevant there. It is in this work that spin correlations are shown to be equally important in understanding the CMR physics that appears in the one-orbital model. Charge and spin correlations develop together at short distances.

To better understand the relation between charge and spin correlations, the following MC simulation in the CMR regime, at  $J_{AF}=0.0325$  and  $\lambda=1.2$ , was carried out. The simulation was initialized with a configuration where the system has charge correlations similar to the AF/CO state. This was achieved by running another simulation with  $J_{AF}=0.05$ ,  $\lambda=1.2$ ,  $T/t=0.01$ , and using the final configuration as the initial configuration in the new run. A snapshot of this initial configuration is presented in Fig. 4(a). During the MC evolution, the oxygen lattice distortions degrees-of-freedom were kept *frozen* to their initial values, but the spins were allowed to change (note that we use one of the equilibrated MC configurations as our “frozen” lattice and there the holes are not regularly distributed as in a perfect CO state. However, the average over many MC configurations at the couplings used do give long-range order in the charge correlations). By freezing the phonons, the charge order is stabilized, and it provides a static inhomogeneous background that is temperature independent. If the spin and charge were decoupled, when cooling the system in the CMR regime, spins can still experience a PM-to-FM transition, and the system may be driven to a metal due to the DE mechanism. However, as shown in Figs. 4(c) and (d), this is not what we obtained from MC simulations. In fact, the system is never driven to a FM state even at very low

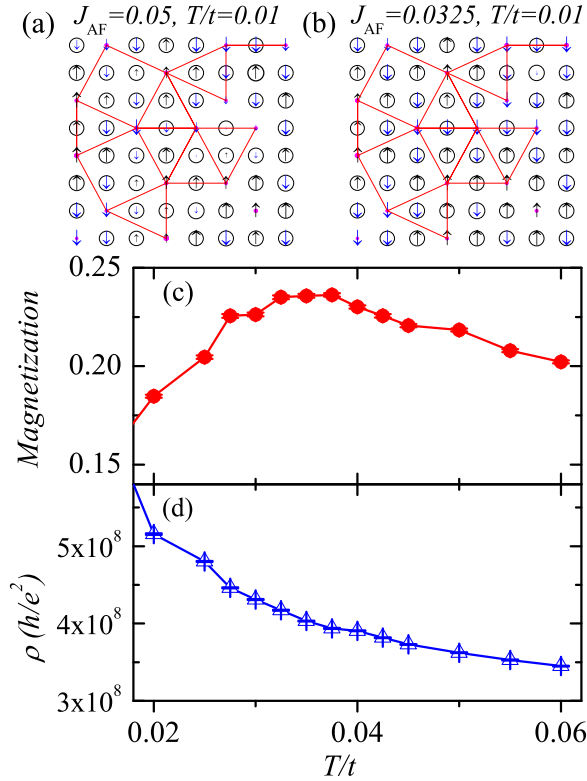


FIG. 4: (color online) MC results obtained by freezing the phononic degree-of-freedom (see text for details). Snapshots of initial and final configurations are shown in (a) and (b), respectively. Also shown are the normalized magnetization (in (c)) and resistivity (in (d)). With frozen charges, the DE mechanism cannot produce the FM state at low temperatures.

temperatures. By observing the final configuration of the MC simulation at  $T/t=0.01$  in Fig. 4(b) and comparing it with the initial one, we find that spins are effectively also frozen if the charges are frozen during the MC evolution. Thus, the system is locked in the AF/CO state. Interestingly, this picture holds even when  $J_{AF}=0$  (not shown). Then, clearly spin flipping processes are greatly suppressed by freezing the charge and lattice distortions. This suggests that: (i) the spin and charge degrees are strongly coupled in the CMR regime; (ii) CMR cannot take place in a quenched inhomogeneous charge background. The CMR is related to a more complex effect: upon cooling across  $T_C$ , the charge order partially melts allowing for a metal to develop.

### C. Dynamical Properties of Charge and Spin Correlations in Monte Carlo Time

In the one-orbital model without quenched disorder being analyzed here, the translation invariance symmetry

cannot be broken unless a state with long-range AF/CO order is stabilized, and this occurs only at low temperatures and sufficiently large  $J_{AF}$ . Then, in the CMR regime where the resistivity peak appears, the MC-time-averaged charge density must be the same at every site. However, in the MC snapshots previously discussed, a short-distance charge localization resembling the AF/CO state leads to a non-uniform distribution of charge  $\langle n_i \rangle$ . Then, as a state without long-range CO but containing strong distortions resembling the AF/CO state, the charge localization in the CMR regime can only be understood in a dynamical context. In other words, even after the MC thermalization that removes the dependence on the initial configuration, in the CMR regime the system is still inhomogeneous at any instant during the simulation, but it slowly becomes homogeneous when averaged over very long MC times. It is, thus, interesting to investigate this dynamics. Note that, in principle, it is not obvious that real-time and MC-time dynamics have any common trends. However, both are based on local events (local interactions in the real system to evolve in real time; local updates in the MC evolution used here). Thus, the expectation is that long-lived metastabilities and tendencies toward glassy behavior and a complex landscape revealed via MC-time studies will have an analog in the real system. To the extent that the analysis in MC time is considered only qualitatively, our expectation is that crude dynamical trends for the real system can be discussed based on a local-update MC-time evolution.<sup>36</sup> With these caveats, here several characteristic MC times, revealing dynamical correlations of the spin and charge degrees-of-freedom in the system, will be numerically analyzed. It will be argued that glassy properties emerge at the CMR regime, and we speculate (but do not prove rigorously) that similar tendencies will occur in real manganites. A variety of experiments showing glassy tendencies indicate that this assumption is realistic.<sup>37</sup>

Consider first the MC-time evolution of the conductance (inset of Fig. 5). In the present type of studies based on calculating the quantum-mechanical transmission to obtain conductances, it is well-known that the conductance is quantized, namely it varies among discrete values due to the presence of an integer number of channels of transmission, from one side to the other of the cluster investigated. The observed “jumps” between two quantized values reflects on changes that occurred in the charge and spin correlations. Thus, the average MC time  $t_G$  that the conductance remains at a certain quantized value provides information about the system MC dynamics. From Fig. 5, it is interesting to observe that  $t_G$  has a very clear peak precisely at the metal-insulator transition temperature. In other words, as the system is cooled down, concomitant with the development of short-range charge and spin correlations, a variety of metastable states develop, as in a glass. The system tends to be trapped in those states and evolving to other states is difficult. Eventually at very low temperatures, deep into the FM state, the metastabilities

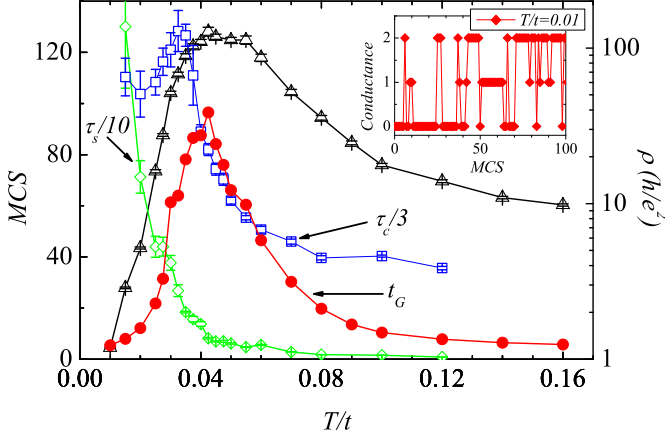


FIG. 5: (color online) Characteristic times that illustrate the spin and charge MC dynamics in the one-orbital model are here shown as a function of temperature, together with the resistivity.  $t_G$  is the average MC time that the conductance  $G$  remains constant at one of its quantized values.  $\tau_c$  is the autocorrelation time of the local charge density.  $\tau_s$  is the autocorrelation time of the uniform spin structure factor. The inset contains typical measurements of the conductance as a function of MC time, illustrating the discrete values it takes.

vanish and the system rapidly evolves in MC time. It is remarkable that  $t_G$  qualitatively follows the shape of the resistivity  $\rho$ . This suggests that the charge localization close to  $T_{MI}$  has glassy characteristics,<sup>37</sup> and if the free energy were available in the CMR regime, it would show a complex landscape of peaks and valleys. The long lifetimes near the CMR resistivity peak show the practical difficulty in achieving true translation invariance: for this to occur, the system must visit dynamically all the many competing arrangements of charge and spin to render the average uniform.

We can also study an autocorrelation time  $\tau_c$  related with the charge. For this purpose, let us define the autocorrelation function  $A(t)$  of the local charge density as

$$A(t) = \frac{\frac{1}{NT_0} \sum_{i=1}^N \sum_{t'=1}^{T_0} [n_i^{t+t'} - \bar{n}_i][n_i^{t'} - \bar{n}_i]}{\frac{1}{NT_0} \sum_{i=1}^N \sum_{t'=1}^{T_0} [n_i^{t'} - \bar{n}_i][n_i^{t'} - \bar{n}_i]}, \quad (5)$$

where  $\bar{n}_i = \frac{1}{T_0} \sum_{t=1}^{T_0} n_i^t$ , and  $T_0$  is the total number of MC steps used in the measurements (50,000 in this case). It was observed that  $A(t)$  decays exponentially as  $A(t) \sim e^{-t/\tau_c}$ , where  $\tau_c$  is the autocorrelation time of the local charge density. The temperature dependence of  $\tau_c$  is also shown in Fig. 5. It has a similar shape as  $t_G$ , indicating that charge has a tendency toward localization in long-lived states near the CMR peak. However, the peak in  $\tau_c$  is shifted to temperatures lower than the metal-insulator transition temperature. Thus, charge localization is still quite stable even below  $T_{MI}$ . This picture changes at very low temperature, where  $\tau_c$  increases again, and the

system stabilizes a metallic state with uniform charge distribution. This increase of  $\tau_c$  at low temperature is unrelated to charge localization, but it reflects on the stable uniformity of the FM state charge distribution.

As discussed above, spin dynamics is also important in understanding the resistivity peak in the CMR regime. Similar to charges, an autocorrelation time can be defined for the spins. This autocorrelation function reads

$$A(t) = \frac{\sum_{t'=1}^{T_0} [S^{t+t'} - \bar{S}][S^{t'} - \bar{S}]}{\sum_{t'=1}^{T_0} [S^{t'} - \bar{S}][S^{t'} - \bar{S}]}, \quad (6)$$

where  $S = \frac{1}{N} \sum_{i,j} \mathbf{S}_i \cdot \mathbf{S}_j$  is the uniform spin structure factor, and  $\bar{S} = \frac{1}{T_0} \sum_{t=1}^{T_0} S$ . The autocorrelation time  $\tau_s$  is then defined through  $A(t) \sim e^{-t/\tau_s}$ . As shown in Fig. 5, it increases quickly at  $T < T_{MI}$  indicating the stabilization of a FM state.

We found that very short-range FM correlations exist even in the AF/CO state. This is clear by observing a typical MC snapshot of spin correlations. In a perfect AF/CO state, each hole is surrounded by four neighbors that have their classical spins parallel to the classical spin on that hole site. As previously discussed, such spin blocks are then antiferromagnetically arranged in the AF/CO state (see Fig. 1(b)). However, if all these block spins align, a FM state is reached. It is then interesting to ask how the spins rotate when experiencing a transition from the short-distance AF/CO state in the CMR regime to the FM state stable at lower temperatures. Do they rotate coherently, behaving as blocks of spins, or the spins rotate more individually one at a time? To clarify this matter, let us study the MC evolution of the average block spin  $|\bar{\mathbf{S}}| = \sqrt{\frac{1}{N} \sum_i \bar{\mathbf{S}}_i^2}$ . Let us also study the average angle between the spin at a hole site and its four nearest-neighboring spins, defined as  $\cos \Theta = \frac{1}{(1-\bar{n})L^2} \sum_{i=\text{holes}} \mathbf{S}_i \cdot \mathbf{S}_{i+\hat{x}}$ . The results are shown in Fig. 6. The MC simulation was performed at low temperature where a FM ground state is finally reached. However, it was started with an initial configuration obtained in an almost perfect AF/CO state.<sup>38</sup> The initial and final configurations have very similar values for  $|\bar{\mathbf{S}}|$ . If the spins rotate incoherently,  $|\bar{\mathbf{S}}|$  should be first reduced substantially and then grow back when a large portion of spins are parallel (to establish the long-range FM order), and  $\cos \Theta$  should be randomly centered around 0. If, on the other hand, spins rotate coherently, both  $|\bar{\mathbf{S}}|$  and  $\cos \Theta$  should remain nearly constant and close to 1 over the MC time evolution. As seen from Fig. 6(a), both quantities converge to their equilibrium values very fast, even before the thermal equilibrium of the FM state is established. It is interesting that both quantities do not change too much during the MC time evolution, which indicates that spins rotate coherently in blocks, at least as a first approximation.

These results would suggest the following picture: although not perfectly, the spins in a block mainly rotate coherently, such that they keep parallel to one another



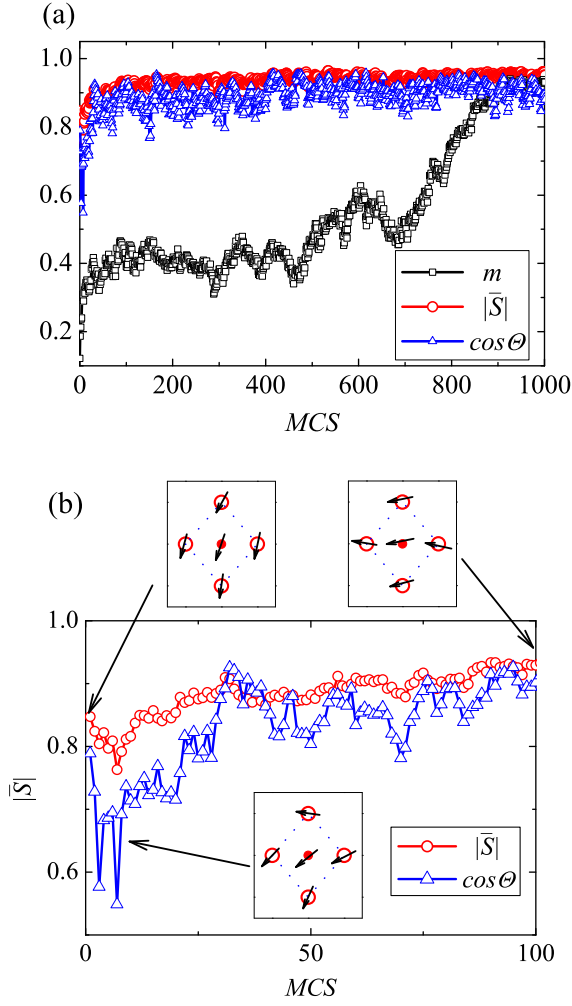


FIG. 6: (color online) (a) MC time evolution of  $|\bar{S}|$ ,  $\cos\Theta$ , and the normalized magnetization  $m$ . The MC simulation is initialized by a configuration with short-distance AF/CO order (similar to that shown in Fig. 1(b)), but the simulation occurs at very low temperature, where a FM ground state is stable (similar to that shown in Fig. 1(a)). (b) MC-time evolution of  $|\bar{S}|$  and  $\cos\Theta$ , at shorter MC-time scales than in (a). Three snapshots of a typical block of spins in the early stages of MC evolution are also shown.

during the MC evolution. This picture is consistent with the charge localization scenario for the AF/CO state, and the MI transition in the CMR regime can be understood in the following way. At  $T > T_{\text{MI}}$ , holes are localized in these local FM spin blocks, and different spin orientations between adjacent blocks suppress inter-block charge transfer, giving the PM phase an insulating nature. However, holes are not frozen at their initial sites. As they travel from site to site, they coherently rotate spins on their neighboring sites in the block. At  $T < T_c \approx T_{\text{MI}}$ , long-range spin correlations establish. Blocks are aligned

in parallel, charges are no longer localized in blocks but can freely move all over the lattice, developing metallic properties. Note the consistency between the above described picture and the “correlated polaron” picture often mentioned in the experimental literature<sup>30</sup> by referring to the local FM blocks around holes as “small polarons”. These polaronic entities are *not* independent but they have tendencies to very particular short-distance arrangements in the CMR regime. This agreement between theory and experiment also supports the view that at least qualitatively the study of MC dynamics provides useful information regarding the actual real time dynamics of manganite compounds.

#### IV. THE LOCAL DENSITY-OF-STATES IN THE ONE-ORBITAL MODEL

Motivated by recent STS experiments,<sup>26,27</sup> we have systematically studied the behavior of the LDOS in the one-orbital model for manganites, with focus on the CMR regime. For this analysis, we have worked on an  $8 \times 8$  lattice with model parameters  $J_{\text{AF}}=0.0325$  and  $\lambda=1.2$ . Before proceeding with the local DOS analysis, note that the site averaged LDOS is just the DOS  $N(\omega)$  of the system. Unlike what the experimental results have suggested recently,<sup>26</sup> we do not observe any *hard* gapped feature in  $N(\omega)$ , at any temperature. However, as shown in Fig. 7, in the CMR regime of the one-orbital model, our results for the DOS present a clear and fairly deep PG centered at the chemical potential, both below and above the critical temperatures. Starting from the high-temperature insulating phase, the DOS at the chemical potential first decreases upon cooling the system, it reaches a minimum at approximately  $T_{\text{MI}}$ , and then grows up again. The temperature dependence of the inverse of the DOS,  $N^{-1}(\omega = \mu)$ , qualitatively follows the shape of the resistivity. An enhancement in  $N^{-1}(\omega = \mu)$  reveals a clear tendency to an insulating state, result compatible with all the previous analysis of transport and spin/charge short-distance correlations. Once spatial fluctuations are included, most features observed in the DOS apply to LDOS as well.

Although a hard gap in the LDOS was not observed in our model even in the insulating phase, we found several similarities between properties of the PG regime and those of a normalized conductance curve reported in experiments.<sup>26</sup> The obvious one is that the PG exists in the full CMR temperature range we studied, both in the FM metallic state and in the PM insulating phase, while in experiments a hard gap is found in both regimes as well. Moreover, in the experiment, the width of the LDOS gap near the chemical potential  $\mu$  was determined. Its temperature dependence was associated with the development of a polaron binding energy. For further comparison with experimental results, we have studied the width of the PG in our LDOS. The local width  $\Delta E_i$  is determined by taking the half-distance between the

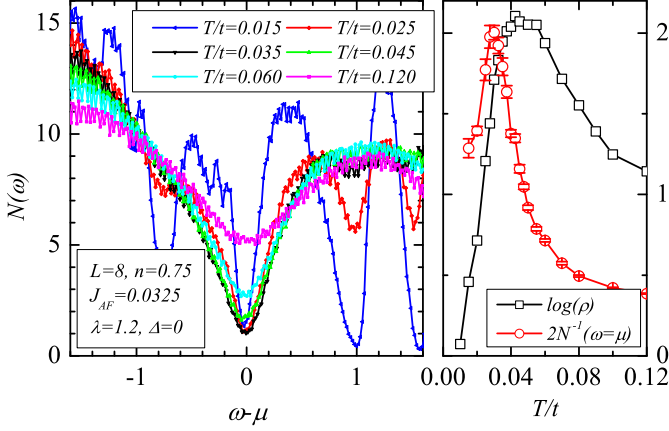


FIG. 7: (color online) *Left*: Density of states  $N(\omega)$  at various temperatures, in the CMR regime. A pseudogap develops in both the PM insulating and FM metallic states. *Right*: temperature evolution of  $N^{-1}(\omega = \mu)$  and the resistivity  $\rho$ .

two peaks that are the closest to the chemical potential, at each lattice site  $i$ . The site-averaged width  $\Delta E$ , its variance  $\sigma_{\Delta E}$ , and the distribution of  $\Delta E_i$ , denoted by  $P(\Delta E_i)$ , are then calculated.

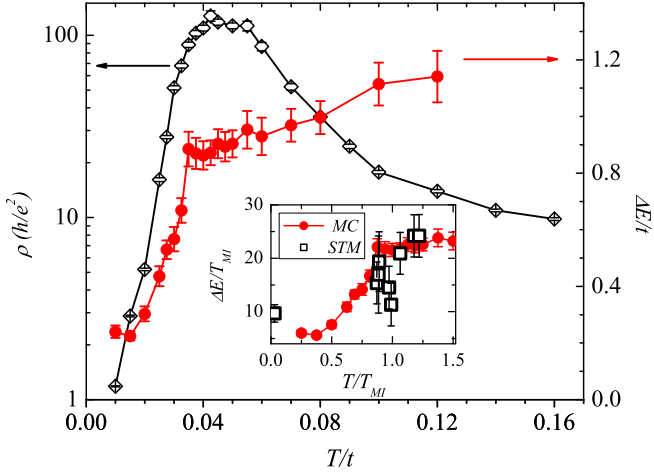


FIG. 8: (color online) Temperature dependence of the site-averaged width  $\Delta E$  of the pseudogap in the LDOS. Also shown is the resistivity (black diamonds) at the same model parameters. *Inset*:  $\Delta E$  rescaled by the critical temperature of the MI transition  $T_{MI}$ . Also shown as black squares are the experimentally determined “polaronic gaps” (extracted from Ref. 26) rescaled by  $T_{MI}$ .

In Fig. 8, the site-averaged width  $\Delta E$  is shown together with the resistivity.  $\Delta E$  has a small value at low temperatures in the FM metallic phase, as expected.

However, this quantity increases upon raising the temperature. Close to  $T \sim T_{MI}$ ,  $\Delta E$  develops a cusp and it flattens into a plateau at about where the resistivity shows a peak. Actually, at exactly  $T \approx T_{MI}$  it reaches a local minimum, namely a little dip on the plateau, but it is difficult to judge if such a small effect can survive the bulk limit. Upon further heating,  $\Delta E$  slowly increases again. To directly compare our results with experimental data, we rescaled  $\Delta E$  and the temperature  $T$  with respect to  $T_{MI}$ . The rescaled dimensionless  $\Delta E$  together with experimental data (rescaled as well) are shown in the inset of Fig. 8. The quantitative agreement is very good in almost the full temperature range. Nevertheless, there is a difference between experiments and our calculation close to  $T \approx T_{MI}$ . Experimentally a notorious dip was observed, but this feature appears to be very weak in our simulations, as already discussed. However, the overall behavior is at least qualitatively the same both in theory and experiments.

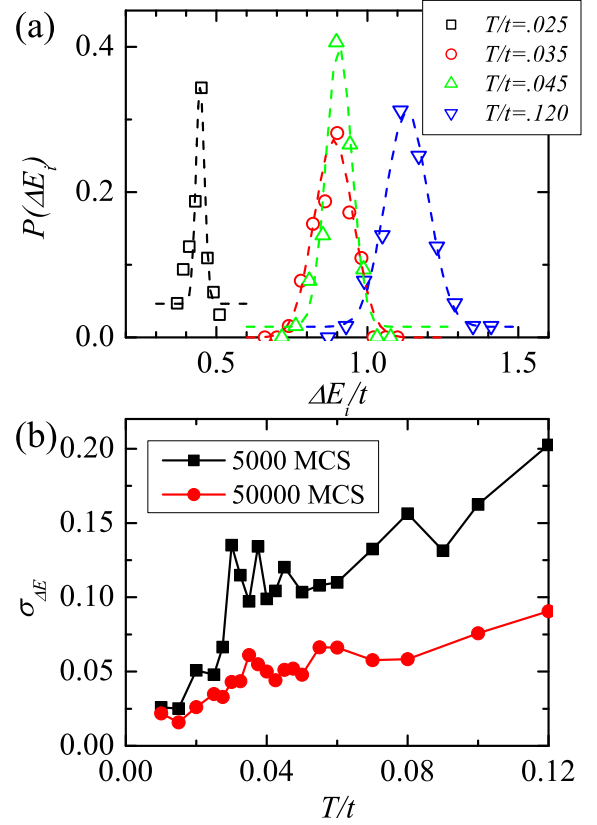


FIG. 9: (color online) Statistics of the width of the LDOS pseudogap  $\Delta E_i$ . (a) A general Gaussian probability distribution of  $\Delta E_i$  at various temperatures in both the FM metallic and PM insulating phases is observed, when MC-averaged over long times. (b) The standard deviations of  $\Delta E_i$ . The system behaves more inhomogeneously in shorter MC-time scales.

As a further comparison, we present the distribution

of LDOS widths,  $P(\Delta E)$ , in the PM insulating phase, as well as in the FM metallic phase. As shown in Fig. 9(a), we have observed that in both phases the distribution can be fitted by a Gaussian, in full agreement with the experimental findings.<sup>26</sup> At first glance, a single-peak Gaussian distribution implies that the system is homogeneous, with no competing metallic and insulating domains. However, we have to emphasize that the distribution in our model is taken from very long MC simulations, similarly as the STS experiment which is “slow” in typical time scales of relevance for electronic systems. Thus, the Gaussian distribution of widths indicates that the system is statistically homogeneous when time averaged. In other words, the site-averaged LDOS PG width,  $\Delta E$ , equals to the PG width of the DOS in a very long MC run. But it does not exclude the possibility of having a dynamical inhomogeneity, such as the charge localization and formation of local FM spin blocks discussed in the previous sections. Since the distribution of the PG width is Gaussian, its variance  $\sigma_{\Delta E}$  is then a measure of the inhomogeneity in the system. This quantity is illustrated in Fig. 9(b):  $\sigma_{\Delta E}$  strongly depends on the number of MC steps in the simulation, especially close to  $T_{\text{MI}}$  in the insulating phase, where the dynamical charge localization and correlations are enhanced. If the number of MC steps for the MC measurements is comparable to the characteristic time of the system dynamics, such as the autocorrelation times  $\tau_c$  and  $\tau_s$ , a different distribution of LDOS PG widths may appear.

Following this idea, we compare the distribution of  $\Delta E_i$  between two MC simulations. These simulations are performed for the same couplings and other parameters, but one is done with  $5 \times 10^4$  MC steps, while the other one has only 100 MC steps (both after  $10^5$  MC steps for thermalization). As shown in Fig. 10(a), the distribution is now quite different: a Gaussian is observed for the long run, but a double-peak distribution, which can be fitted by a superposition of two Gaussian’s, applies to the short run. The real space images in Fig. 10(b) and (c) further confirm that the system looks more inhomogeneous at very short time scales. For the same reason, if one were able to perform the STS experiment in a much shorter time scale than currently possible, namely with times comparable to characteristic relaxation times in the system, then a different gap distribution revealing the intrinsic dynamical inhomogeneity would be observed in the experiment.

It is important to further discuss this surprising agreement between our calculation and the STS experiments. While it is easy to imagine a gapped spectrum in an insulator, finding a gap in the metallic phase seems very unusual. The explanation proposed in Ref. 27 is clearly a possibility, namely the surface behaves differently than the bulk. However, if the concept of a hard gap is replaced by the pseudogap, then another possible scenario appears. A PG in the metal renders the system a “bad metal”, as observed experimentally since the values of the resistivity are high in the low temperature phase. Find-

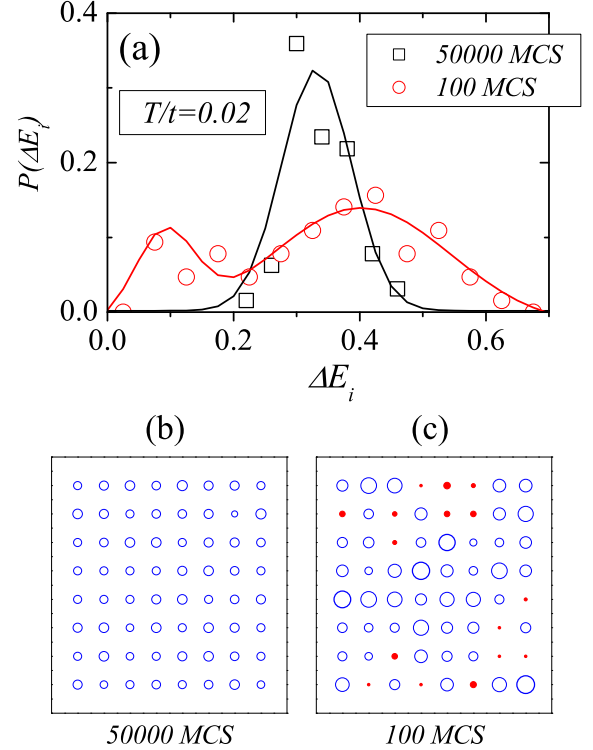


FIG. 10: (color online) (a) Distribution of the width of the LDOS pseudogap  $\Delta E_i$  at different MC time scales. Real space images of  $\Delta E_i$  measured under 50,000 and 100 MC steps at  $T/t = 0.02$  are also provided in (b) and (c), respectively. The radius of each circle is proportional to the local  $\Delta E_i$  value at that site. Open circles corresponds to  $\Delta E_i/t \geq 0.2$ , whereas solid (red) ones corresponds to  $\Delta E_i/t < 0.2$ .

ing charge approximately localized and correlated in the FM metallic state near the MI transition is not too surprising, according to the physical picture and results we have discussed in previous sections. It is then natural to explain the STS gapped feature of the conductance spectrum observed experimentally as a result of a fairly deep PG, which cannot be distinguished experimentally from a hard gap. In retrospect this is fairly obvious: a hard gap cannot exist in a metal. But for a PG coexisting with bad metallic properties, there is no contradiction.

## V. CONCLUSION

In conclusion, we have investigated the MI transition in the CMR regime, and the associated PM to FM transition, using the one-orbital model with cooperative oxygen lattice distortions and superexchange coupling  $J_{\text{AF}}$ , at electronic density  $n = 0.75$ . Both the resistivity and magnetization are continuous as a function of tempera-

ture, indicating a second order phase transition. However, strong tendencies to develop spin and charge short-range order were observed. It has been shown that the tendency toward the AF/CO state at short-distances accounts for the appearance of the sharp resistivity peak at the critical Curie temperature. Robust charge localization and correlations exist in both the insulating and metallic phases, and are enhanced in the temperature range where a resistivity peak exists. Charge localization together with correlations in the spin and charge degrees-of-freedom are shown to be dynamical, at least with respect to the MC time in the simulations, which can be characterized by autocorrelation times  $\tau_c$  and  $\tau_s$ . The model studied here presents properties in the CMR regime that resemble a glassy system.

We have also studied the LDOS of the one-orbital model in the CMR regime. A PG is observed at all temperatures. The width of this PG, together with the variance and distribution of the width, are calculated and compared with results from a recent STS experiment. To our surprise, given the crudeness of the calculations, theory and experiments agree not only qualitatively, but in some cases even quantitatively. This study provides an explanation to the puzzling STS experimental results, suggesting that the gapped features in the normalized conductance spectrum observed in the STS experiment

actually originates from a pseudogap. We also point out that the observed homogeneity in STS investigations may reflect on the time-averaged properties of the system. The system is actually dynamically inhomogeneous, at least in our Monte Carlo time evolution. Our prediction is that experimental techniques that are fast, namely with time scales comparable to the system's intrinsic dynamics in the CMR regime, should see indications of the widely expected nanoscale phase separation. However, slow techniques, such as STS, should observe an homogeneous state in the same regime.

## VI. ACKNOWLEDGEMENT

We thank S. Seiro and S. Yunoki for useful discussions. Work supported by the NSF grant DMR-0706020 and the Division of Materials Science and Engineering, U.S. Department of Energy, under contract with UT-Battelle, LLC. A portion of this research at Oak Ridge National Laboratory's Center for Nanophase Materials Sciences was sponsored by the Scientific User Facilities Division, Office of Basic Energy Sciences, U.S. Department of Energy. S. D. is also supported by the China Scholarship Council (2007U03040).

- 
- <sup>1</sup> C. N. R. Rao and B. Raveau, eds., *Colossal Magnetoresistance, Charge Ordering, and Related Properties of Manganese Oxides* (World Scientific, Singapore, 1998).
  - <sup>2</sup> Y. Tokura, *Colossal Magnetoresistive Oxides* (Gordon and Breach, New York, 2000).
  - <sup>3</sup> E. Dagotto, T. Hotta, and A. Moreo, *Physics Reports* **344**, 1 (2001).
  - <sup>4</sup> E. Dagotto, *Science* **309**, 257 (2005).
  - <sup>5</sup> M. B. Salamon and M. Jaime, *Rev. Mod. Phys.* **73**, 583 (2001).
  - <sup>6</sup> A. P. Ramirez, *Science* **315**, 1377 (2007); E. Dagotto, *Science* **318**, 1076 (2007); and references therein.
  - <sup>7</sup> C. Zener, *Phys. Rev.* **81**, 440 (1951); C. Zener, *ibid.*, **82**, 403 (1951).
  - <sup>8</sup> A. Millis, P. Littlewood, and B. Shraiman, *Phys. Rev. Lett.* **74**, 5144 (1995).
  - <sup>9</sup> M. Calderón, J. Vergés, and L. Brey, *Phys. Rev. B* **59**, 4170 (1999).
  - <sup>10</sup> A. Millis, B. Shraiman, and R. Mueller, *Phys. Rev. Lett.* **77**, 175 (1996).
  - <sup>11</sup> S. Yunoki, J. Hu, A. Malvezzi, A. Moreo, N. Furukawa, and E. Dagotto, *Phys. Rev. Lett.* **80**, 845 (1998).
  - <sup>12</sup> A. Moreo, S. Yunoki, and E. Dagotto, *Science* **283**, 2034 (1999).
  - <sup>13</sup> E. Dagotto, *Nanoscale Phase Separation and Colossal Magnetoresistance* (Springer Verlag, Berlin, 2002).
  - <sup>14</sup> J. Burgý, M. Mayr, V. Martín-Mayor, A. Moreo, and E. Dagotto, *Phys. Rev. Lett.* **87**, 277202 (2001).
  - <sup>15</sup> M. Mayr, G. Alvarez, and E. Dagotto, *Phys. Rev. B* **65**, 241202 (2002).
  - <sup>16</sup> J. Burgý, A. Moreo, and E. Dagotto, *Phys. Rev. Lett.* **92**, 097202 (2004).
  - <sup>17</sup> J. Vergés, V. Martín-Mayor, and L. Brey, *Phys. Rev. Lett.* **88**, 136401 (2002).
  - <sup>18</sup> S. Kumar and P. Majumdar, *Phys. Rev. Lett.* **94**, 136601 (2005).
  - <sup>19</sup> S. Kumar and P. Majumdar, *Phys. Rev. Lett.* **96**, 016602 (2005); *Phys. Rev. Lett.* **94**, 136601 (2005). See also P. Majumdar and S. Kumar, *J. Phys. Soc. Jpn. Suppl.* **74**, 216 (2005); S. Kumar, A. Kampf, and P. Majumdar, *Phys. Rev. B* **75**, 014209 (2007); S. Kumar and A. Kampf, arXiv:0706.1425.
  - <sup>20</sup> J. Salafranca and L. Brey, *Phys. Rev. B* **73**, 214404 (2006).
  - <sup>21</sup> C. Şen, G. Alvarez, H. Aliaga, and E. Dagotto, *Phys. Rev. B* **73**, 224441 (2006).
  - <sup>22</sup> C. Şen, G. Alvarez, and E. Dagotto, *Phys. Rev. Lett.* **98**, 127202 (2007).
  - <sup>23</sup> In the clean limit, experimental results have confirmed that the phase diagram of manganites contains a first-order transition separating the FM metallic and AF/CO insulating phases (see Y. Tomioka and Y. Tokura, *Phys. Rev. B* **70**, 014432 (2004)).
  - <sup>24</sup> M. Fäth, S. Freisem, A. A. Menovsky, Y. Tomioka, J. Aarts, and J. A. Mydosh, *Science* **285**, 1540 (1999).
  - <sup>25</sup> C. Renner, G. Aeppli, B.-G. Kim, Y.-A. Soh, and S.-W. Cheong, *Nature* **416**, 518 (2002).
  - <sup>26</sup> S. Seiro, Y. Fasano, I. Maggio-Aprile, E. Koller, O. Kuffer, and Ø. Fischer, *Phys. Rev. B* **77**, 020407 (R) (2008).
  - <sup>27</sup> U. R. Singh, S. Chaudhuri, S. K. Choudhary, R. C. Budhani, and K. Gupta, arXiv: cond-mat/0712.1017.
  - <sup>28</sup> A. Moreo, S. Yunoki, and E. Dagotto, *Phys. Rev. Lett.* **83**, 2773 (1999).

- <sup>29</sup> Photoemission studies in bilayered manganites have shown the existence of a pseudogap in these materials in the CMR regime. See D. S. Dessau, T. Saitoh, C.-H. Park, Z.-X. Shen, P. Villeda, N. Hamada, Y. Moritomo, and Y. Tokura, *Phys. Rev. Lett.* **81**, 192 (1998); N. Mannella, W. L. Yang, X. J. Zhou, H. Zheng, J. F. Mitchell, J. Zaanen, T. P. Devereaux, N. Nagaosa, Z. Hussain, and Z.-X. Shen, *Nature* **438**, 474 (2005).
- <sup>30</sup> P. Dai, J. A. Fernandez-Baca, N. Wakabayashi, E. W. Plummer, Y. Tomioka, and Y. Tokura, *Phys. Rev. Lett.* **85**, 2553 (2000); C. P. Adams, J. W. Lynn, Y. M. Mukovskii, A. A. Arsenov, and D. A. Shulyatev, *Phys. Rev. Lett.* **85**, 3954 (2000); and references therein. More information about “correlated polarons”, which can also be called charge-ordered nanoclusters, and neutron scattering results showing the coexistence of FM and AF tendencies above the FM critical temperature can be found in Chapter 19 of Ref. 13. See also J. M. De Teresa, M. R. Ibarra, P. A. Algarabel, C. Ritter, C. Marquina, J. Blasco, J. Garca, A. del Moral, and Z. Arnold, *Nature* **386**, 256 (1997); and Z. Sun, J. F. Douglas, A. V. Fedorov, Y.-D. Chuang, H. Zheng, J. F. Mitchell and D. S. Dessau, *Nature Physics* **3**, 248 (2007).
- <sup>31</sup> The important role of  $J_{AF}$  was discussed in S. Yunoki and A. Moreo, *Phys. Rev. B* **58**, 6403 (1998) and J. L. Alonso, L. A. Fernandez, F. Guinea, V. Laliena, and V. Martin-Mayor, *Phys. Rev. B* **63**, 064416 (2001); **63**, 054411 (2001).
- <sup>32</sup> For instance, see Figs. 1, 3, and 6(a) of Ref. 21; and references therein.
- <sup>33</sup> J. A. Vergés, *Comp. Phys. Commun.* **118**, 71 (1999); and references therein.
- <sup>34</sup> According to Ref. 20, the transition should turn into first order when the strength of quenched disorder exceeds a certain critical value. In future work, it will be interesting to study the MI transition in the model with quenched disorder, and numerically check the validity of this analytical claim.
- <sup>35</sup> In practice, hole sites are defined as sites with the lowest  $(1 - n)L^2$  local densities of states at each MC step, where  $n$  is the number of electrons in a  $L \times L$  system.
- <sup>36</sup> If the MC evolution were carried out using non-local updates (using, e.g., cluster updates), then the analogy between the real system and the MC evolution is lost.
- <sup>37</sup> The presence of glassy states in manganites has been discussed in a variety of contexts already. See for instance F. Parisi, P. Levy, L. Ghivelder, G. Polla, and D. Vega, *Phys. Rev. B* **63**, 144419 (2001); D. N. Argyriou, J. W. Lynn, R. Osborn, B. Campbell, J. F. Mitchell, U. Ruett, H. N. Bordallo, A. Wildes, and C. D. Ling, *Phys. Rev. Lett.* **89**, 036401 (2002); D. Akahoshi, M. Uchida, Y. Tomioka, T. Arima, Y. Matsui and Y. Tokura, *Phys. Rev. Lett.* **90**, 177203 (2003); R. Mathieu, D. Akahoshi, A. Asamitsu, Y. Tomioka, and Y. Tokura, *Phys. Rev. Lett.* **93**, 227202 (2004); H. Aliaga, D. Magnoux, A. Moreo, D. Poilblanc, S. Yunoki, and E. Dagotto, *Phys. Rev. B* **68**, 104405 (2003); Y. Motome, N. Furukawa, and N. Nagaosa, *Phys. Rev. Lett.* **91**, 167204 (2003). More information about glassy behavior in manganites can be found in Chapter 13 of Ref. 13.
- <sup>38</sup> The simulation is performed at  $T/t = 0.01$  with  $J_{AF} = 0.0325$  and  $\lambda = 1.2$ , where a metallic FM state is finally stabilized. However, in this simulation the initial configuration is prepared by taking the final configuration of another long MC simulation in the AF/CO state (with  $J_{AF} = 0.05$ ,  $\lambda = 1.2$ , and  $T/t = 0.01$ ).